Shear-induced structure in polymer blends with viscoelastic asymmetry

E. K. Hobbie,[a] H. S. Jeon,[b] H. Wang, H. Kim,[c] D. J. Stout,[d] and C. C. Han
National Institute of Standards and Technology, Gaithersburg, Maryland 20899

(Received 8 April 2002; accepted 9 July 2002)

Light scattering and optical microscopy have been used to measure the morphology as a function of shear rate and composition in polymer blends with viscoelastic asymmetry in the melt components. The blends studied are immiscible mixtures of low-vinyl polybutadiene (PB) and high-vinyl polyisoprene (PI), where the vinyl content strongly influences the rheological properties of the melt. At the temperatures where the optical measurements described here were performed, the PI starts to exhibit an elastic response above a critical shear rate $\dot{\gamma}_c$, while the PB responds like a viscous fluid up to the highest shear rates of interest. The disparate rheology of the two fluids leads to a rich variety of domain patterns and orientations as the volume fraction of the more elastic component is varied. © *2002 American Institute of Physics.* [DOI: 10.1063/1.1503769]

I. INTRODUCTION

Due to the relatively small entropy of mixing of most macromolecular pairs, many polymer mixtures of practical interest are immiscible, and mixing devices are often used to emulsify or *blend* the two components.[1] During processing, such blends often form emulsionlike distributions of one melt phase dispersed in another, and the properties and characteristics of the ensuing two-phase polymeric material are influenced, sometimes quite strongly, by the shape and size of the droplets, as well as the relative rheological properties of the droplet (dispersed) phase and the matrix (continuous) phase. Although the flow fields encountered in practical mixing devices are complex, the local velocity field at a given point within the mixing device often contains a component of simple shear flow [with the flow direction defined along the *x* axis, a constant velocity gradient along the *y* axis, and the neutral (vorticity) direction along the *z* axis]. This relatively simple flow field is unique in that it contains equal amounts of pure elongation and pure rotation.

As fluids, polymer melts often exhibit dramatic non-Newtonian behavior, and studies of polymer blends under simple shear flow also provide valuable and fundamental insight into the physics of multiphase viscoelastic fluids. Small-angle light scattering has proven to be a valuable tool for measuring the shear response of immiscible polymer blends,[2–7] and real-space microscopy is emerging as a powerful tool for directly visualizing droplets and domains in polymer blends under shear.[8–10] A limited number of recent studies have combined both light scattering and optical microscopy *in situ* to probe the shear response of polymer blends under realistic processing conditions.[10–15] In some of these mixtures, the shear flow homogenizes the fluid back to a thermodynamically homogeneous (miscible) state at sufficiently high shear rates ($\dot{\gamma}$). In this paper, we describe light-scattering and optical-microscopy measurements of the domain morphology as a function of shear rate and composition in immiscible polymer blends with viscoelastic asymmetry in the melt components. The blends studied are mixtures of low-vinyl polybutadiene (PB) and high-vinyl polyisoprene (PI), where the vinyl content strongly influences the rheological properties of the melt. At 130 °C, where the optical measurements described here were performed, the PI exhibits an elastic response above a critical shear rate $\dot{\gamma}_c$, while the PB responds essentially as a viscous fluid up to the highest shear rates of interest. The disparate viscous and elastic properties of the two melt components leads to a rich variety of domain shapes and anisotropies as the shear rate and composition are varied.

II. MATERIALS AND METHODS

A. Materials

The polymers used in this study were synthesized at the Goodyear Tire and Rubber Company.[16] The number-averaged relative molecular mass (M_n), the mass-averaged relative molecular mass (M_w), and the polydispersity were determined by gel permeation chromatography, and the microstructure was probed using ^{13}C nuclear magnetic resonance. The polymer chains are statistical copolymers composed of 1–4, 1–2 isomers and 1–4, 3–4 isomers, respectively. The PB has a mole fraction of 1–2 isomers equal to 0.1, while the PI has a mole fraction of 3–4 isomers equal to 0.9. In general, $M_n = 51\,000$ and $M_w/M_n = 1.04$ for the PB, while $M_n = 72\,000$ and $M_w/M_n = 1.02$ for the PI. These two polymers are immiscible over the range of temperatures accessible to the instrument.[14] The blends were prepared via solution blending from methylene chloride (mass fraction of polymer in solution = 0.02) containing the appropriate amount of each component and a small amount (mass fraction of 0.0005 in solution) of Goodyear Wingstay #29 antioxidant. The mixture was stirred at room tempera-

[a]Electronic mail: erik.hobbie@nist.gov
[b]Also at the Department of Petroleum and Chemical Engineering, New Mexico Institute of Mining and Technology, Socorro, New Mexico 87801.
[c]Also at the Department of Chemistry, Kyunghee University, Yongin, Kyungkido, 449-701 Korea.
[d]Also at the Departments of Chemistry and Chemical Engineering, University of California, Irvine, California 92697.

ture for 1 day and filtered through a 0.45 μm Gelman Acrodisc CR PTFE filter. The solvent was then evaporated under an atmosphere of flowing nitrogen gas, and the sample was dried in a vacuum oven at room temperature for several days. All shear experiments were performed at 110–140 °C. The samples were heated from room temperature and annealed for 30 min before shearing to obtain a reproducible initial two-phase morphology for each sample.

B. Instrumentation

The *in situ* scattering/microscopy instrument, capable of collecting two-dimensional light scattering data and real-time microscopy images in the flow/vorticity (x-z) plane, was designed and constructed for conducting optical measurements of complex fluids under simple shear flow.[17] The sample compartment is composed of two electrically heated quartz plates, and the temperature of each plate is controlled to within ± 0.5 K by a 100 Ω platinum-resistance-temperature-detector (RTD) element in conjunction with a 1 mA current source. The gap between the plates typically varied from 200–500 μm. A beam of vertically polarized monochromatic light from a 15 mW He–Ne laser (wavelength $\lambda = 632.8$ nm) was directed through the sample. The image of the scattered light in the angular range 4°–27° (with respect to the incident beam) [corresponding to wave vector (q) values ranging from 0.6 to 4.5 μm^{-1}] was focused onto a thermoelectrically cooled two-dimensional charge-coupled-device (CCD) detector using a pair of spherical condensers, and the array of data from the 256×256 pixel CCD camera was then transferred to a personal computer. The microscope image is collected with a different CCD camera (Dage MTI, model 72), recorded onto a super-VHS tape, and digitized using a frame grabber from Data Translation (DT 3851). Conventional bright field microscopy relies on a significant refractive index difference between the two phases to resolve the image. In the case of phase-separated PB/PI blends, the refractive index difference between the two components is small ($n_{PB} = 1.512$ and $n_{PI} = 1.517$),[18] and the phase-separated blends are not optically turbid. Phase-contrast microscopy was thus used in addition to bright-field microscopy to image the morphology. An advantage of this small optical contrast, however, is that multiple scattering effects are suppressed when light scattering is used to probe the structure. A strobe flash synchronized with the video frame acquisition provides clean sharp images at high shear rates. A Rheometrics Scientific SR-5000 rheometer in both cone-and-plate and parallel-plate geometry was used for dynamic measurements of the linear viscoelasticity and steady-shear measurements of the viscosity, shear stress, and first normal stress difference,[19] which were carried out with 25 mm diameter fixtures and a (0.4 ± 0.01) mm gap thickness. The temperature was controlled to within ± 0.5 K, and the measurements were carried out under a nitrogen atmosphere to prevent any thermal degradation of the polymers, which are known to be heat sensitive.

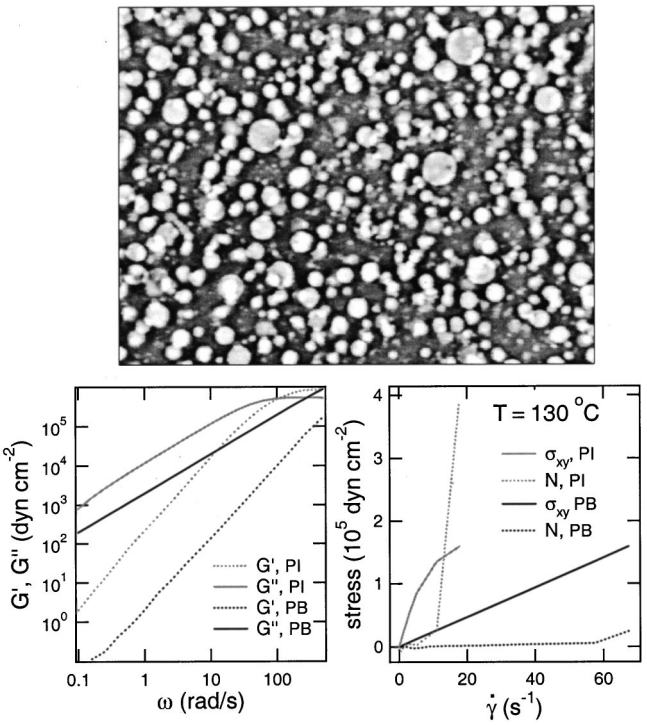

FIG. 1. Spherical PI droplets dispersed in a continuous PB phase ($\dot{\gamma} = 0$, 130 °C) for $\phi = 0.10$, where the width of the micrograph is 200 μm. The lower left figure shows $G'(\omega)$ (dash) and $G''(\omega)$ (solid) for the PI (gray) and PB (black) at 130 °C. The lower right figure shows σ_{xy} (solid) and N (dash) of the PI (gray) and PB (black) as a function of shear rate at 130 °C.

III. RESULTS AND DISCUSSION

A. Melt rheology

The quiescent blends typically coarsen into emulsionlike dispersions consisting of spherical droplets of one phase dispersed in the other, as shown in the upper panel of Fig. 1. The PI volume fraction is denoted ϕ. From an extrapolation based on small-angle-neutron-scattering measurements, we estimate that the mixtures exhibit upper-critical-solution-temperature (UCST) behavior with a spinodal temperature that is much greater than the upper limit of any meaningful (both instrumentally and materially) range of temperatures.[14] Because of the (hypothetical) UCST coexistence curve, slight thermodynamic mixing might occur in the presence of shear in either one of the dilute limits, where the transition temperature might be low enough to fall in the vicinity of the relevant temperatures. In this study, however, we assume that any true mixing that occurs under shear is negligible. Specifically, we focus on $0.02 \leqslant \phi \leqslant 0.40$, and $\phi = 0.80$ at $T = 130$ °C. In the first blends, the PI forms the dipersed phase, while in the latter, the PB forms the (quiescent and weak shear) dispersed phase.[14]

The effect of the shear field is to distort and break up the droplets, and the specific shear response depends strongly on the rheology of both the dispersed and continuous phases. In Fig. 1, the lower-left panel shows the loss modulus (G'') and the storage modulus (G') as a function of angular frequency (ω), and the lower-right panel shows the shear stress (σ_{xy}) and the normal stress difference (N) as a function of shear rate ($\dot{\gamma}$) for each of the two melts at 130 °C. The shear-

viscosity ratio (η_{PI}/η_{PB}) is 10 in the $\dot{\gamma}\to 0$ limit, although the PI exhibits shear thinning (as evidenced by a deviation from linear behavior in σ_{xy} versus $\dot{\gamma}$) and this ratio approaches 4 in the limit of high shear stress. Asymmetry is also present in the elasticity. In the PB, G'' exceeds G' over the entire range of ω, while in the PI, G' exceeds G'' at $\omega_c \approx 100$ rad/s, implying that elastic forces emerge in the PI over a range of shear rates where viscous forces remain dominant in the PB. From a Maxwell model of linear viscoelasticity,[19] we can obtain a measure of the dynamic asymmetry via a relaxation time $\tau=\lim_{\omega\to 0} G'/(\omega G'')$, which at 130 °C is of order 0.0015 and 0.02 s for the PB and PI, respectively. The elasticity of the PI can also been seen in the steady-shear measurements, where N exceeds σ_{xy} at a critical shear rate $\dot{\gamma}_c \approx 15\ s^{-1}$. As discussed in detail below, evidence of an elastic response in the blends starts to emerge at shear rates in the vicinity of 10 s^{-1}, and in this paper we focus on the collective behavior of concentrated blends in the regime $0.5<\dot{\gamma}/\dot{\gamma}_c<7$, where internally generated elastic forces are an important factor in the response.[9] Equivalently, but perhaps more fundamentally, we measure the blend response in the regime $0.1<De<2$, where $De=\tau\dot{\gamma}$ is the Deborah number of the PI melt at 130 °C (assuming $\tau \approx 0.02$ s).

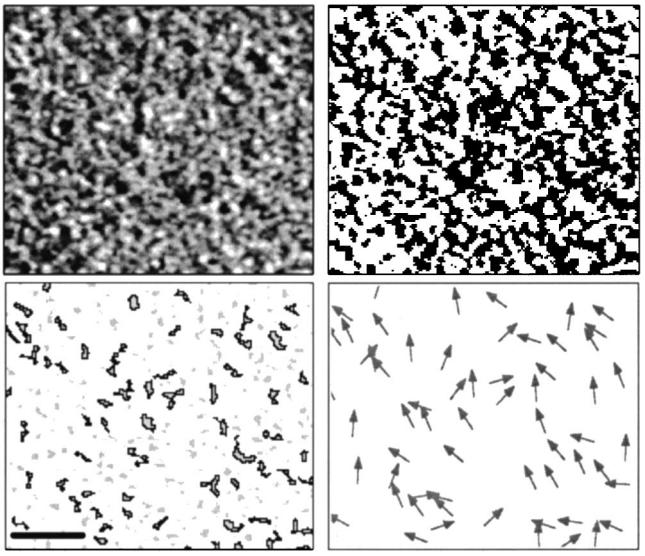

FIG. 2. A typical micrograph ($\phi=0.20$, $\dot{\gamma}=75\ s^{-1}$), with the flow ($\hat{\mathbf{x}}$) direction to the right and the vorticity ($\hat{\mathbf{z}}$) direction from bottom to top. The real-space image (upper left) yields a binary image (upper right) of the distorted PI domains (black) in the continuous PB phase (white). Further thresholding preserves only the brightest regions (lower left, outlined in black, scale bar=25 μm), where the orientation of the outlined shapes is used to extract the local director field (lower right) that gives the orientation of the domains.

B. Computational background

The morphology can be quantified with both real-space image analysis and small-angle light scattering. By thresholding the digitized micrographs into binary black and white, we obtain approximate slices of the binary PI–PB domain morphology in the flow–vorticity plane.[20] From these modified images, the two-point composition correlation function,

$$c_{kl}=\left\langle A^{-1}\sum_{ij}\ \phi_{ij}\phi_{i+k,j+l}\right\rangle, \tag{1}$$

is computed from the field ϕ_{ij}, where ϕ_{ij} (=1 or 0) is the PI composition of pixel ij. The indices i and k denote pixel number along the x axis, j and l denote pixel number along the z axis, and $A=\Sigma_{ij}\phi_{ij}$ is the effective area of the image. For example, an image with $\phi_{ij}=1$ for all i and j gives $c_{kl}=1$ for all k and l. For $k=l=0$, Eq. (1) gives $c(0)=1$. In the limit of large k and l, the pixel values become uncorrelated, and Eq. (1) reduces to the area fraction of the image. In computing this correlation function, results obtained from a number of images taken at different depths within the sample are averaged together at a given shear rate and composition, and this ensemble average, represented by the brackets in Eq. (1), is assumed to give an accurate representation of the projection of the full three-dimensional two-point correlation function,

$$c(\mathbf{r})=\left\langle V^{-1}\int d\mathbf{r}'\ \phi(\mathbf{r}')\phi(\mathbf{r}'+\mathbf{r})\right\rangle, \tag{2}$$

in the flow–vorticity plane. Projections of this two-dimensional version of $c(\mathbf{r})$ onto the appropriate axes can then be used to extract a measure of the mean domain size and shape. Computations of $c(\mathbf{r})$ were performed with both periodic and box boundary conditions with no ascertainable difference in the results. The correlation functions displayed here have been renormalized to decay to zero at large separations.

The image processing procedure is depicted in Fig. 2, where the image corresponds to $\phi=0.20$ at a shear rate of 75 s^{-1}. The micrograph (upper left) is thresholded and inverted into a binary image (upper right) that reveals distorted PI domains (black) in a continuous PB phase (white). This modified image is a two-dimensional slice of the three-dimensional morphology[20] and gives a map of the local composition field $\phi(\mathbf{r})$. The steady-state structure consists of locally connected domains oriented at various angles with respect to the flow field, reminiscent of the behavior reported by Moses *et al.*,[21] who used real-space image analysis to quantify tilted "ripple waves" in sheared polymer solutions. To quantify the domain orientation in the blend for $0.02 \leqslant \phi \leqslant 0.40$, we measure the local tilt angle with respect to the vorticity direction by further thresholding the image so that only the brightest (largest) domains of the original micrograph survive (gray regions, lower-left panel, Fig. 2). Of these, only those with an area greater than 13 μm^2 (outlined in black) are used to obtain a measure of the director field $\theta(\mathbf{r})$ (lower right panel, Fig. 2), where the cutoff ensures that only long-wavelength fluctuations are used in the analysis. To measure $\theta(\mathbf{r})$, a threshold level was chosen that gave an average of $n=200$ bright regions above the cutoff per image (200×150 μm) at $\phi=0.20$. As a function of ϕ, the level was then varied with respect to this reference such that $n \propto \phi^{2/3}$. The computer algorithm defines the orientation of a region as the axis that yields the smallest moment of inertia, and the director field is mapped out by placing a unit vector with this orientation at the centroid of the region.

If the distribution of domains is random, then a linear

slice of $\phi(\mathbf{r})$ along an arbitrary axis resembles a collection of dilute, randomly spaced square waves of random width. The autocorrelation along that direction is then an exponential decay, with a decay constant equal to half the characteristic pulse width.[22] Under shear flow, domain–domain interactions are important in all but the dilute limit, and thus the locations of the PI–PB interfaces are in fact not random. Indeed, for certain compositions and shear rates, $c(\mathbf{r})$ exhibits well-defined minima, or correlation holes, reminiscent of weak (anisotropic) liquidlike order. This is not exclusively the case, however, and to obtain a consistent measure of the effective domain size, we fit the data in the $|\mathbf{r}|\rightarrow 0$ limit to the approximate expression

$$c(\mathbf{r}) \approx \exp\{-2r\alpha(\hat{\mathbf{n}})\}, \tag{3}$$

where $R(\hat{\mathbf{n}})=1/\alpha(\hat{\mathbf{n}})$ provides a measure of the spatial coherence along the direction $\hat{\mathbf{n}}=\mathbf{r}/r$ as a function of composition and shear rate. A particularly simple form of $\alpha(\hat{\mathbf{n}})$ is one with ellipsoidal anisotropy;

$$\alpha(\hat{\mathbf{n}})^2=\sum_{i=1}^{3} \hat{\mathbf{n}}\cdot\hat{\mathbf{x}}_i/R_i^2. \tag{4}$$

The structure factor measured in reciprocal space with small-angle light scattering, $S(\mathbf{q})$, is the Fourier transform of $c(\mathbf{r})$. With the above expression for $\alpha(\hat{\mathbf{n}})$, the Fourier transform of Eq. (3) can be easily computed to obtain the static structure factor

$$S(\mathbf{q}) \propto R_x R_y R_z \left[1+\left(\frac{q_x R_x}{2}\right)^2+\left(\frac{q_y R_y}{2}\right)^2+\left(\frac{q_z R_z}{2}\right)^2\right]^{-2}. \tag{5}$$

Equation (5) is the anisotropic analog of the expression originally derived by Debye for the scattering from random, isotropic, sharp interfaces,[23] and fitting the light-scattering data to Eq. (5) in the large-q limit provides an additional measure of the domain size and shape. The length scales determined from these fits, however, are typically a factor of 2 smaller than those determined directly from $c(\mathbf{r})$, although the anisotropy and shear-rate dependence are the same. Such disagreement is to be expected, however, as Eq. (3) is only an asymptotic approximation and thus does not represent the full form of $c(\mathbf{r})$. As discussed in greater detail below, a common feature of the measured light-scattering pattern is the presence of winglike lobes (''butterfly'' patterns) that are intimately linked to correlation holes in $c(\mathbf{r})$. These correlation minima are in turn intimately related to interactions, reflecting a weak periodicity in the location of the interfaces. Such effects are ignored by Eq. (3). In this paper we present data obtained in both real and reciprocal space, but the quoted domain dimensions are determined from the real-space images via fitting the projections to $c(x_i) \approx \exp(-2x_i/R_i)$ in the $x_i\rightarrow 0$ limit.

C. $0.02 \leqslant \phi \leqslant 0.40$

As discussed above, measurements of the melt rheology suggest that internal elastic forces start to emerge in the vicinity of a critical shear rate, $\dot{\gamma}_c$. When the PI is the dispersed phase, such internally generated normal forces lead to the extension of isolated droplets along the vorticity direction.[9] As shown in Fig. 3, this effect is already evident in the optical data collected for $\phi=0.20$ at $\dot{\gamma}=8\ \mathrm{s}^{-1}$ ($\dot{\gamma}/\dot{\gamma}_c \approx 0.53$). Although no minima are evident in $c(\mathbf{r})$, the real-space data exhibit slight anisotropy with mean elongation along the vorticity direction. To eliminate any residual anisotropy in $c(\mathbf{r})$ associated with slight off-axis illumination in the micrographs, correlation functions have been made symmetric with respect to the vorticity direction. As shown in the lower panel of Fig. 3, the light scattering pattern at $\dot{\gamma}=8\ \mathrm{s}^{-1}$ exhibits a weak crease along the vorticity axis. At $\dot{\gamma}=75\ \mathrm{s}^{-1}$ ($\dot{\gamma}/\dot{\gamma}_c \approx 5$, real-space images shown in Fig. 2), two distinct lobes are clearly evident in the light scattering pattern (Fig. 4). The cartoon at the bottom of Fig. 4 depicts a

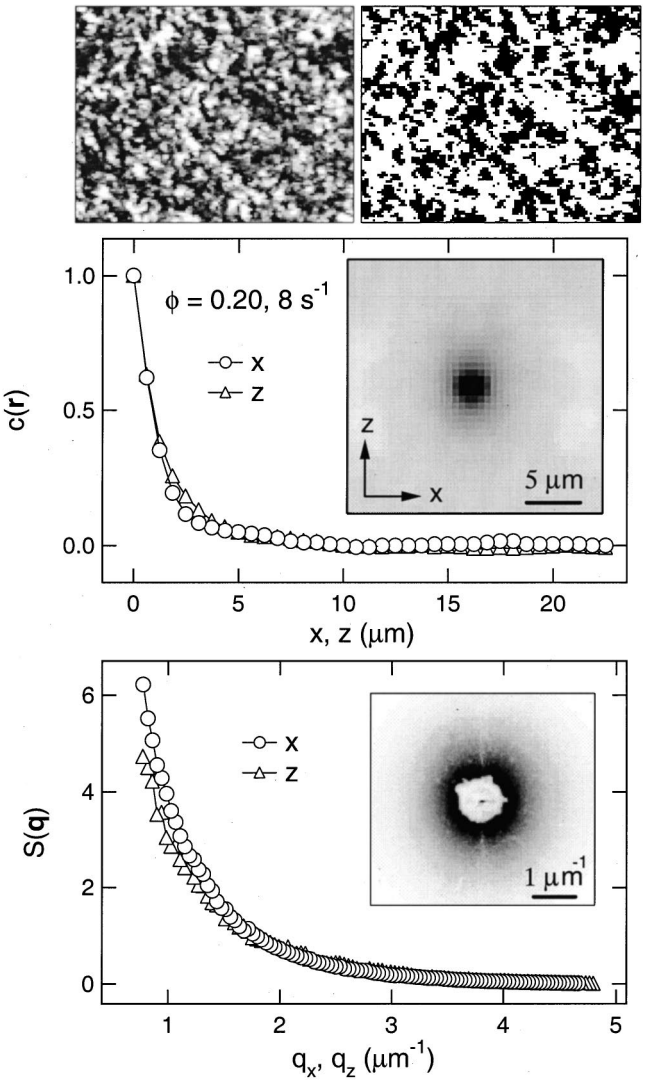

FIG. 3. Morphology of a blend with $\phi=0.20$ at the intermediate shear rate of 8 s^{-1}. The width of the micrograph (upper left) is 75 μm, with the flow direction along the horizontal axis and the vorticity direction along the vertical axis. Thresholding and binarizing the image resolves the two phases (upper right), where the black regions are PI and the white regions are PB. From the binary images, the two-point correlation function in the x-z plane, $c(\mathbf{r})$, is computed (inset, middle). The origin of the anisotropy is discussed in the text. The middle graph shows projections of $c(\mathbf{r})$ onto the flow (x) and vorticity (z) directions. The lower figure shows the small-angle light scattering pattern $S(\mathbf{q})$ (inset) and projections of $S(\mathbf{q})$ onto the x and z axes.

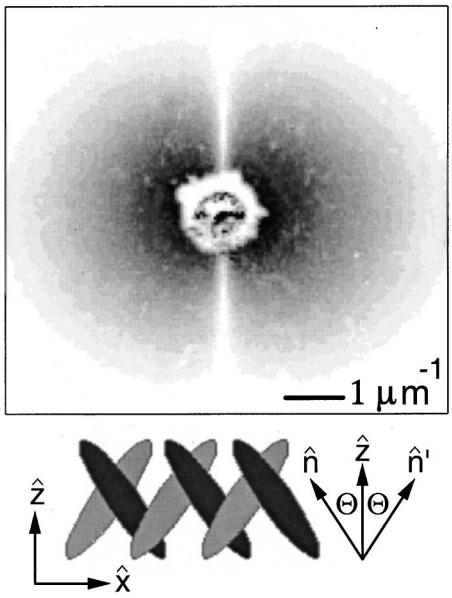

FIG. 4. Light-scattering pattern for the data in Fig. 2 ($\phi=0.20, \dot{\gamma}=75\ s^{-1}$), where the flow ($\hat{\mathbf{x}}$) and vorticity ($\hat{\mathbf{z}}$) directions are as indicated. The bottom panel shows a crude cartoon of the domain morphology, where the tilt angle Θ (defined below) serves as a useful parameter for characterizing the response. The symmetry of this broadly tilted morphology with respect to the vorticity and flow directions can be inferred from the symmetry of the light-scattering patterns.

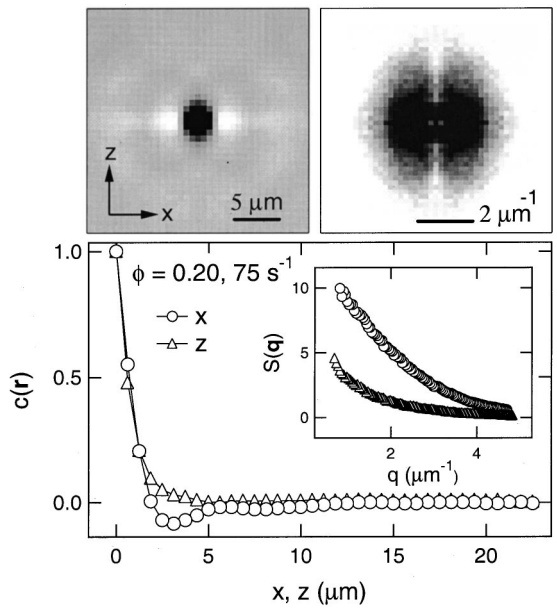

FIG. 5. The upper left panel shows the two-point correlation function, $c(\mathbf{r})$, computed for the data in Fig. 2. The upper right panel shows the Fourier transform of $c(\mathbf{r})$, which closely resembles the light-scattering pattern, $S(\mathbf{q})$, in Fig. 4. The main panel shows projections of $c(\mathbf{r})$ and $S(\mathbf{q})$ (inset) along the flow and vorticity directions. Weak minima along the flow direction in $c(\mathbf{r})$ gives rise to the winglike structure of $S(\mathbf{q})$ in Fig. 4.

tilted morphology of the distorted PI domains with respect to the flow geometry, where the physical significance of the angle $\Theta=\cos^{-1}(\hat{\mathbf{n}}\cdot\hat{\mathbf{z}})$ follows from an analysis of the real-space images (e.g., Fig. 2) and is discussed in more detail below. The symmetry of the morphology with respect to the vorticity axis, however, can be inferred from the symmetry of the light-scattering pattern. The upper-left panel of Fig. 5 shows the two-point correlation function, $c(\mathbf{r})$, for the data depicted in Fig. 2, while the upper right panel shows its Fourier transform, which reproduces the distinct lobelike features of the measured light-scattering pattern in Fig. 4. Projections of $c(\mathbf{r})$ along the flow and vorticity directions are shown in the main panel of Fig. 5, while the inset shows similar projections of $S(\mathbf{q})$. The well-defined minima along the flow direction at $x\approx 3\ \mu$m, apparent as light correlation holes in $c(\mathbf{r})$, are what give rise to the winglike lobes in $S(\mathbf{q})$ and indicate anisotropic ordering in the presence of the shear field.

From the field $\theta(\mathbf{r})$, we compute the tilt-angle distribution function, $p(\theta)$. The inset to Fig. 6(a) shows how $p(\theta)$ varies with ϕ in the regime of interest ($\dot{\gamma}/\dot{\gamma}_c>1$). When $p(\theta)$ is broadly peaked about the vorticity direction, we define Θ as the cutoff in the distribution with respect to the maximum at $\theta=0$. When $p(\theta)$ is bimodal, exhibiting symmetric peaks on either side of $\theta=0$, we define Θ as the peak position. This tilt angle (Θ) serves as a useful parameter for characterizing the response. Because the blends are nearly isorefractive, slight off-axis illumination greatly enhances the contrast in the images and increases the strength of the signal.[24] For $\Theta<\pi/4$, histograms can be obtained from two different oblique measurements [gray solid and dashed curves in Fig. 6(a)] that each emphasize one of the two orientations $\hat{\mathbf{n}}$ or $\hat{\mathbf{n}}'$. The superposition of these two asymmetric subdistributions then provides a measure of the full symmetric $p(\theta)$ (black curve) that is in good agreement with $p(\theta)$ measured with symmetric illumination.[24] The advantage of this technique, however, is that the subdistributions allow a more precise measurement of Θ, since they exhibit a well-defined peak in the vicinity of the cutoff. For $\Theta>\pi/4$, two peaks are sufficiently far apart to be resolved in a single symmetric measurement of $p(\theta)$, as shown in the inset to Fig. 6(a) for $\phi=0.30$ at $75\ s^{-1}$. Figure 6(a) shows the azimuthally averaged tilt–tilt correlation function,

$$g_\theta(r)=\langle\exp\{2i[\theta(\mathbf{r})-\theta(0)]\}\rangle \tag{6}$$

(where the factor of 2 reflects invariance under $\theta\rightarrow\theta\pm\pi$) for the data represented in Figs. 2, 4, and 5 ($\phi=0.20$ and $\dot{\gamma}=75\ s^{-1}$). The solid curve is $g_\theta(r)\sim\exp(-r^2/\xi_\theta^2)$ with $\xi_\theta\approx 100\ \mu$m. Similar correlation lengths were obtained over the entire range of ϕ and $\dot{\gamma}$ of interest. Also shown in Fig. 6(a) is the radial distribution function, $g(r)$, computed from the centroids of the regions used to map $\theta(\mathbf{r})$ at the same composition and shear rate. Within a scale factor, the two correlation functions are similar, implying that the tilt coherence is long range and the spatial decay over ξ_θ reflects the finite image size. Although the tilt distributions are broad, the presence of a peak ensures that $g_\theta(r)$ approaches a constant as $r\rightarrow\infty$.

That the flow orients the domains is not surprising, but the evolution of $\Theta(\phi)$ is intriguing and warrants further consideration. Figure 6(b) shows Θ as a function of ϕ and reduced shear rate ($\dot{\gamma}/\dot{\gamma}_c$), and the inset shows $\Theta(\phi)$ at $\dot{\gamma}/\dot{\gamma}_c=3.33$. The data suggest that $\Theta\rightarrow\pi/2$ as ϕ increases. This is also evident in the light-scattering patterns. With increasing

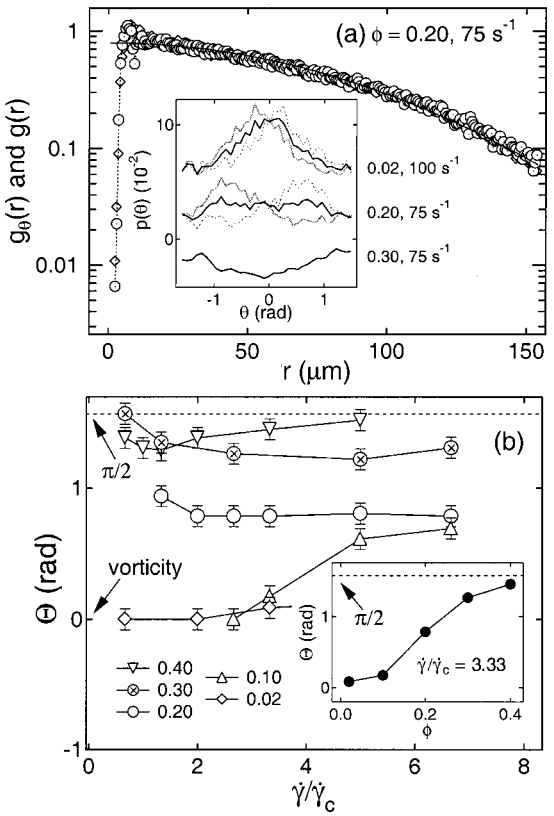

FIG. 6. (a) The correlation functions $g_\theta(r)$ (circles) and $g(r)$ (diamonds) for $\phi=0.20$ and $\dot{\gamma}=75\ \mathrm{s}^{-1}$. The inset shows $p(\theta)$ for $\phi=0.02$, 0.20, and 0.30 in the strong-shear regime ($\dot{\gamma}=100$, 75, and 75 s^{-1}, respectively), where the black curves are a superposition of the two asymmetric subdistributions (solid and dashed gray curves), as described in the text. The data for each composition have been offset by a constant value of 5 for clarity. (b) Θ vs $\dot{\gamma}/\dot{\gamma}_c$ for different ϕ, where the dashed horizontal line indicates the flow direction. The inset shows $\Theta(\phi)$ at $\dot{\gamma}/\dot{\gamma}_c=3.33$.

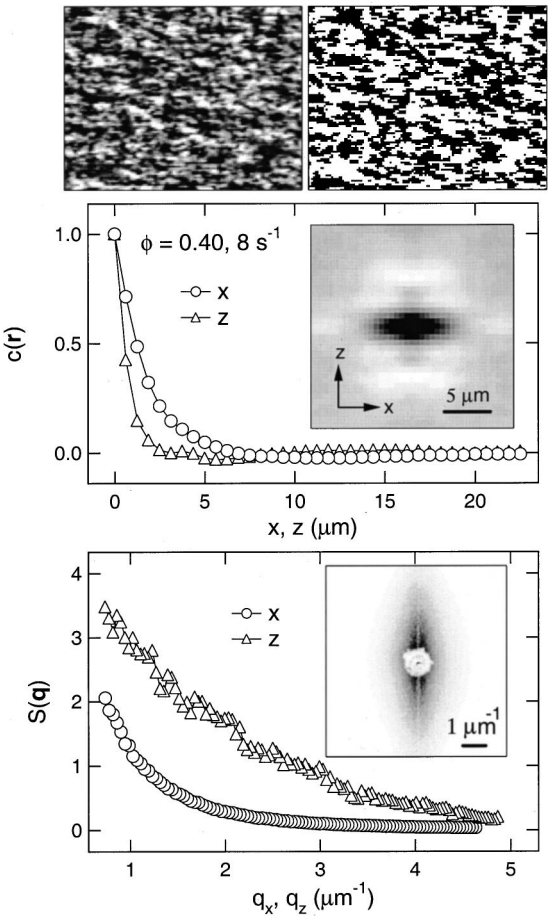

FIG. 7. A plot similar to Fig. 6 for $\phi=0.40$. Increasing the PI volume fraction leads to significant changes in morphology associated with a tighter packing of domains. At an intermediate shear rate ($8\ \mathrm{s}^{-1}$) the behavior can be compared with that exhibited in Fig. 6. Apparent asymmetry associated with the elasticity of the dispersed phase is still present in $c(\mathbf{r})$, although the orientation is now more closely aligned with the flow direction (inset, middle). In the middle figure, $c(\mathbf{r})$ has been projected along the x and z directions. Correspondingly, the light-scattering pattern reflects domains with a large component of elongation along the flow direction, but a subtle crease along the z direction is present.

ϕ, the two wings retract along $\hat{\mathbf{x}}$ and expand along $\hat{\mathbf{z}}$ until they eventually merge. This trend can be seen by comparing the structure exhibited in Fig. 3 ($\phi=0.20, \dot{\gamma}=8\ \mathrm{s}^{-1}$) with that exhibited in Fig. 7 ($\phi=0.40, \dot{\gamma}=8\ \mathrm{s}^{-1}$). This asymptotic behavior is somewhat similar to the measured orientation of rigid rods under shear,[25] suggesting one possible physical explanation. By increasing the volume fraction of the elastic phase, one increases the packing fraction of domains and hence the magnitude of domain–domain interactions. In the dilute limit, the droplets (which respond elastically to high rates of strain yet are inherently soft) elongate and rupture along the vorticity axis. As ϕ increases, weakly repulsive nearest-neighbors interactions mediated by the shear along the direction of flow lead to the weak liquidlike order in Fig. 5. If the packing associated with this order provides a degree of enhanced structural integrity, then the domains might respond like rigid rods, aligning in the vicinity of the direction of flow. For $\phi=0.40$, the distribution of domain orientations suddenly becomes isotropic at a shear rate of 100 s^{-1}, as evidenced by the isotropy of both $c(\mathbf{r})$ and $S(\mathbf{q})$ in Fig. 8. Within the physical picture of semirigid domains, this might reflect the onset of a higher-order ''tumbling'' instability.

D. $\phi=0.80$

At a PI volume fraction of approximately 0.55, the quiescent phase structure inverts; for $\phi<0.55$, the continuous phase is PB, while for $\phi>0.55$, the continuous phase is PI.[14] When the droplet phase is much less viscous than the continuous phase, isolated droplets form stable filamentlike structures under simple shear.[26] At a PI volume fraction of 0.80, the intermediate-shear morphology is stringlike, as shown in Fig. 9. The stringlike pattern is characterized by an extended correlation along the flow direction and weak oscillatory order along the vorticity direction (middle panel, Fig. 9). This asymmetry is inverted in q space (bottom panel, Fig. 9), with reduced scattering along the flow direction and enhanced scattering along the vorticity direction. At higher shear rates, however, the nature of the domain pattern changes, as shown in Fig. 10 for $\dot{\gamma}=100\ \mathrm{s}^{-1}$. The stringlike morphology disappears and is replaced by that depicted in the upper panels of Fig. 10. The two-point correlation function associated with this structure exhibits unusual behavior,

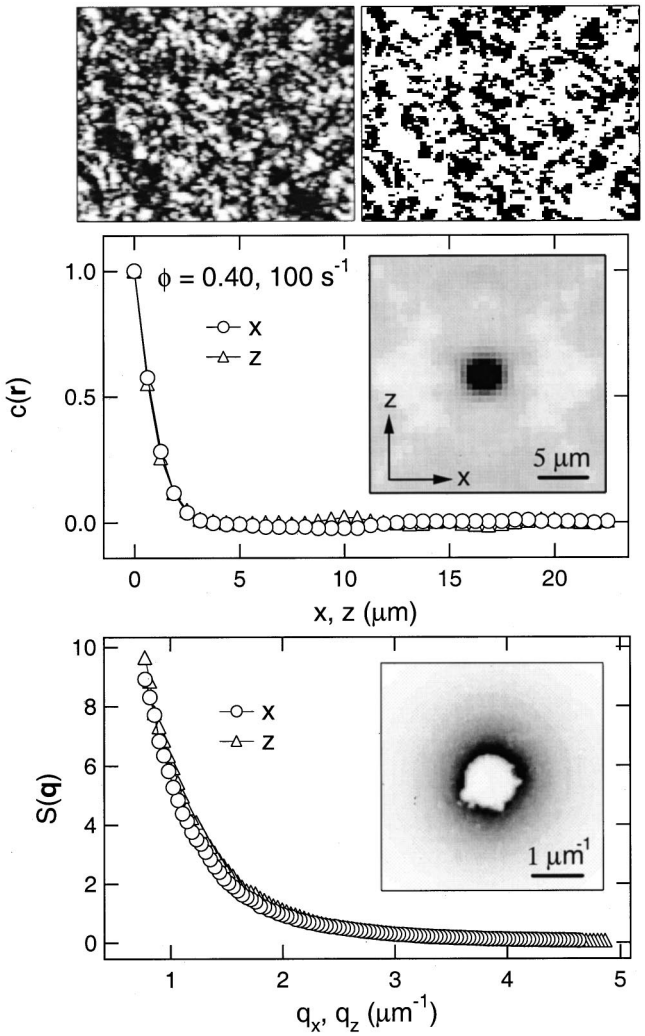

FIG. 8. At a higher shear rate (100 s^{-1}), the domains at $\phi=0.40$ are still significantly deformed, but the distribution of orientations appears to be somewhat random, as indicated by the nearly isotropic shape of $c(\mathbf{r})$ and $S(\mathbf{q})$. In terms of the physical picture of semirigid domains, this onset of isotropy might reflect a crossover from an oriented geometry to a tumbling geometry.

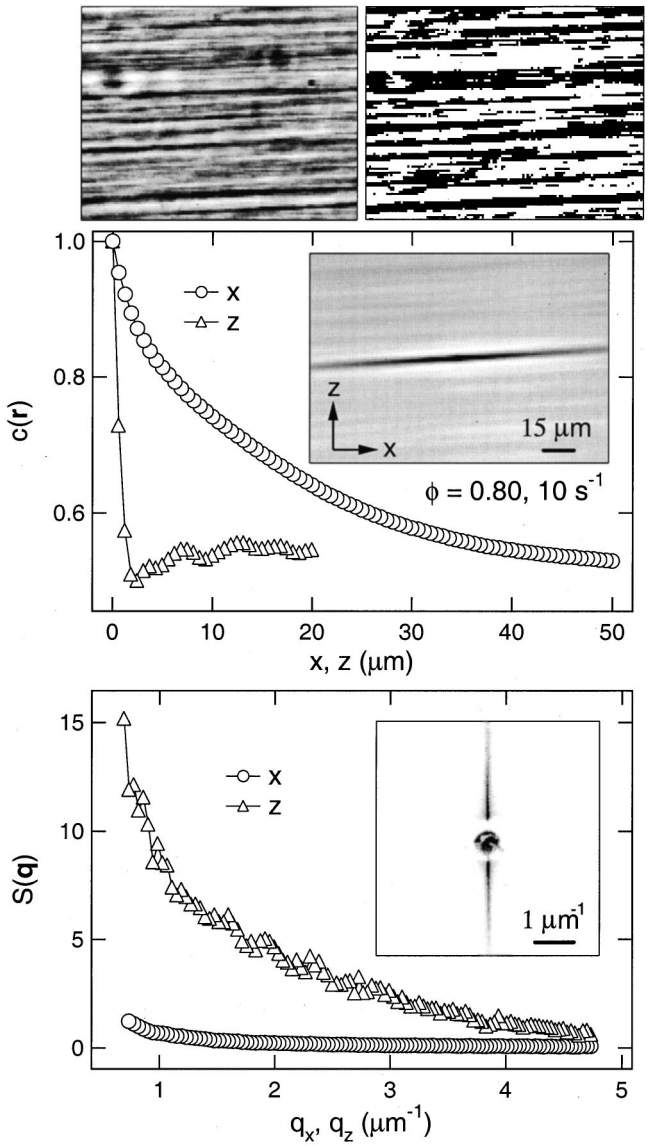

FIG. 9. For $\phi=0.80$ at $\dot{\gamma}=10\ s^{-1}$, the dispersed phase is PB, the matrix is PI, and the morphology is stringlike. The stringlike pattern is characterized by extended correlation along the flow direction and oscillatory order along the vorticity direction (middle). This asymmetry is inverted in q space (bottom), with reduced scattering along the flow direction and enhanced scattering along the vorticity direction.

in that the anisotropy is extended along the flow direction for small displacements, while for larger displacements the behavior is reminiscent of that seen in Fig. 5. This is also evident in the light-scattering pattern, which is a superposition of the light-scattering patterns in Figs. 4 and 9. One explanation for this is a shear-induced phase inversion in which the continuous phase inverts from the more viscous majority PI to the less viscous minority PB. Although such a transition would make sense as a way of efficiently redistributing the shear stress from the viscous to the less viscous phase, this possibility warrants further experimental and theoretical study.

IV. CONCLUSIONS

The results of this work are summarized in Fig. 11, which shows the domain size and anisotropy as a function of shear rate and composition. As stated in Sec. III B, these values are obtained directly from the real-space correlation functions within the approximation of an exponential decay at short distances, which provides a direct and consistent measure of the morphology. The trends are supported by the light-scattering data. In Fig. 11(a) ($\phi=0.20$) the trend is one of gradual breakup with increasing shear rate. For incompressible fluids, the mean dimension decreases by roughly a factor of $2^{-1/3}$ every time the domains rupture, implying that the data in Fig. 11(a) suggest domains that have ruptured two to three times over the range of shear rates in question. Within this regime, the mean component of elongation along the vorticity direction is consistently larger than that along the flow direction, although in reality the domains are broadly tilted with respect to the geometry of the flow field.

In Fig. 11(b), an analogous plot is shown for $\phi=0.40$. With the exception of the highest shear rate, the mean anisotropy is reversed at this volume fraction, with the mean component of elongation along the flow direction being larger

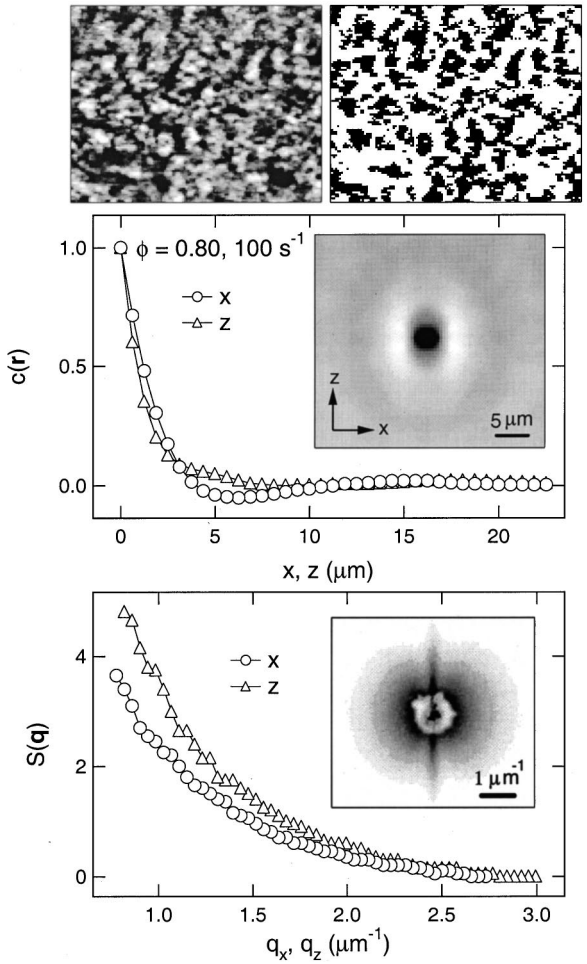

FIG. 10. At $\dot{\gamma}=100\,\mathrm{s}^{-1}$, the morphology of the $\phi=0.80$ sample has changed in a manner that suggests the presence of PI droplets dispersed in a PB matrix, as can be seen by comparing $c(\mathbf{r})$ with that obtained for $\phi=0.20$ in the limit of strong shear (Fig. 5). The middle panel shows a projection of $c(\mathbf{r})$ along the x and z directions. The light-scattering pattern (bottom) is a superposition of a butterfly pattern and a vertical streak.

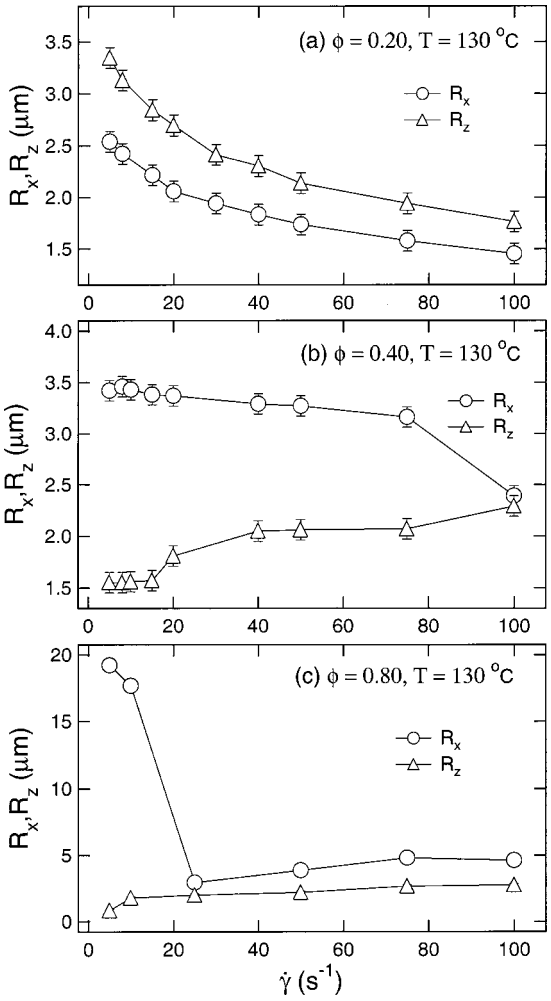

FIG. 11. Domain dimensions (correlation lengths) as a function of shear rate for three different PI volume fractions at 130 °C, where the dimensions are obtained from projections of $c(\mathbf{r})$ onto the axes of flow and vorticity. For $\phi=0.20$ (a), vorticity elongation persists, with slightly decreasing aspect ratio, as the domains become smaller with an increasing shear rate. For $\phi=0.40$ (b), the domains are more oriented along the flow direction. As the shear rate increases, the mean dimension along x decreases while the mean dimension along z increases, until the morphology becomes essentially isotropic at 100 s^{-1}. For $\phi=0.80$ (c), the domains are stringlike along x at low $\dot{\gamma}$, with a transition at around 20 s^{-1}, after which the size is relatively insensitive to shear.

than that along the vorticity direction. The detailed nature of the morphology is the same as for $\phi=0.20$, however, with an overall tilt with respect to the geometry of the flow field. The change in anisotropy from (a) to (b) reflects the fact that the tilt angle Θ increases with increasing volume fraction. As suggested above, one possible physical explanation for this is that as the volume fraction increases, interactions increase in magnitude, which provides a degree of enhanced structural integrity to the domains, implying that they start to respond more like semirigid rods and orient with the flow field. At this point, such an argument is purely heuristic. The onset of an isotropic response at a shear rate of around 80–100 s^{-1} is clearly evident in Fig. 11(b), and such behavior might be indicative of the onset of a ''tumbling'' regime.

For $\phi=0.80$ [Fig. 11(c)], the response up to a shear rate of around 20 s^{-1} is just as would be expected for a viscous continuous phase supporting a dispersion of a much less viscous fluid, in that the morphology is stringlike along the direction of flow. Above this shear rate, however, the behavior is less well understood. That the anisotropy contains a component of elongation along the flow direction is evident in Fig. 10. The anisotropy is inverted for slightly larger displacements, however, where weak minima reminiscent of those depicted in Fig. 5 are evident. As noted above, we suggest that this is strong evidence for a shear-induced phase inversion, although such a scenario is difficult to verify experimentally, in part because the polymers at an ambient temperature are not glassy and conventional temperature-quench microscopy measurements cannot be performed. Rheological measurements of the shear response of the $\phi=0.80$ blend are difficult to interpret. The shear viscosity of the blend (not shown) starts to decrease at $\dot{\gamma}\approx 10\,\mathrm{s}^{-1}$, which would be consistent with the onset of a regime of inversion to a matrix of lower viscosity. However, the shear viscosity of the pure PI melt enters a regime of shear thinning over the same range of shear rate, and the two effects are difficult to decouple. In a dynamic measurement of the linear viscoelas-

ticity of the blend, both the loss and storage modulus increase up to a plateau at an angular frequency of around 20 rad/s, suggestive of the onset of a new response mechanism. The shear thinning of the PI phase could, at least in principle, be the source of this transition as well. At a shear rate of roughly 18 s^{-1}, the PI has shear thinned to the extent that the viscosity ratio of PB to PI would be roughly 0.25. Although this is still significantly less than 1, we cannot rule out the possibility that the behavior depicted in Fig. 10 simply reflects a continuous phase that has shear thinned to the extent that it has become less viscous than the minority phase. The observed morphology, however, is not consistent with what one might expect from this intuitively, in light of the fact that associated with the shear thinning is a large increase in the elasticity of the PI, which should further stabilize stringlike domains.[27] Computational work, as well as measurements performed on a similar blend whose components are glassy at an ambient temperature, would perhaps shed more light on this.

Multiphase fluids with macromolecular components are an intriguing, important, and broad class of soft condensed matter. When subjected to stresses induced by shear flow, the response of such mixtures depends strongly on a number of factors, including the viscoelasticity of the components, the interfacial tension between the phases, the proximity to a critical point, and the presence of a surfactant. Semidilute entangled polymer solutions, for example, exhibit shear-induced phase separation,[21,28–30] while the shear typically has a homogenizing effect on phase-separating polymer blends,[31] which can form stringlike patterns in the presence of the flow field.[10–12,32,33] The addition of modest amounts of block–copolymer surfactant, however, can lead to shear-induced order[34] and shear-induced turbidity[35] in such blends, and a universal understanding of the shear response of these fluids, although highly desirable from both a pure and applied perspective, is clearly a daunting and challenging task. In light of this complexity, limiting scenarios in which one factor plays a dominant role may serve as useful pieces of a comprehensive picture. One particularly interesting example of this can be found in mixtures of viscoelastically disparate components, for which dynamical asymmetry leads to unique phase-ordering kinetics and morphologies.[36–39] In this paper, we have attempted to demonstrate the richness and complexity of the response of such asymmetric mixtures to a simple shear flow, and we hope that this work will help motivate a deeper understanding of this behavior in systems of both scientific and technological relevance.

ACKNOWLEDGMENTS

The authors would like to thank Goodyear Tire and Rubber Company for providing the polymers and A. I. Nakatani for useful discussions regarding the interpretation of the data and assistance with the rheology measurements.

[1] See, for example, L. A. Utracki, *Polymer Alloys and Blends* (Hanser, New York, 1990).
[2] H. Yang, H. Zhang, P. Moldenaers, and J. Mewis, Polymer **39**, 5731 (1998).
[3] J. Vermant, P. Van Puyvelde, P. Moldenaers, J. Mewis, and G. Fuller, Langmuir **14**, 1612 (1998).
[4] H. Gerard, J. S. Higgins, and N. Clarke, Macromolecules **32**, 5411 (1999).
[5] A. Silverburg and W. Kuhn, J. Polym. Sci. **13**, 21 (1954).
[6] T. Takebe, R. Sawaoka, and T. Hashimoto, J. Chem. Phys. **91**, 4369 (1989).
[7] T. Hashimoto, T. Takebe, and K. Asakawa, Physica A **194**, 338 (1993).
[8] L. Levitt, C. W. Macosko, and S. D. Pearson, Polym. Eng. Sci. **36**, 1647 (1996).
[9] F. Mighri and M. A. Hureault, J. Rheol. **45**, 783 (2001); K. B. Migler, *ibid.* **44**, 277 (2000); E. K. Hobbie and K. B. Migler, Phys. Rev. Lett. **82**, 5393 (1999).
[10] T. Hashimoto, K. Matsuzuka, E. Moses, and A. Onuki, Phys. Rev. Lett. **74**, 126 (1995).
[11] L. Kielhorn, R. H. Colby, and C. C. Han, Macromolecules **33**, 2486 (2000).
[12] S. Kim, E. K. Hobbie, J. Yu, and C. C. Han, Macromolecules **30**, 8245 (1997).
[13] H. S. Jeon and E. K. Hobbie, Phys. Rev. E **63**, 061403 (2001).
[14] H. S. Jeon, A. I. Nakatani, E. K. Hobbie, and C. C. Han, Langmuir **17**, 3087 (2001).
[15] Z. Hong, M. T. Shaw, and R. A. Weiss, Polymer **41**, 5895 (2000); Z. Hong, M. T. Shaw, and R. A. Weiss, Macromolecules **31**, 6211 (1998).
[16] In this paper, materials, instruments, and services are specified in order to give a detailed account of the work and do not imply an endorsement by NIST or the Federal Government.
[17] S. Kim, J.-W. Yu, and C. C. Han, Rev. Sci. Instrum. **67**, 3940 (1996). A somewhat similar shear apparatus has been reported by K. Matsuzaka and T. Hashimoto, *ibid.* **70**, 2387 (1999).
[18] J. Brandrup and E. H. Immergut, *Polymer Handbook*, 3rd ed. (Wiley-Interscience, New York, 1989), Chap. IV, p. 455.
[19] See, for example, R. B. Bird, R. C. Armstrong, and O. Hassager, *Dynamics of Polymeric Liquids* (Wiley, New York, 1987), Vol. 1.
[20] Because of the finite depth of field of the measurement, this composition slice is approximate. The thresholding procedure defines the interface to be a specified intensity level between 1 and 256. It provides a meaningful measure when the domain dimensions are the same order of magnitude as the depth of focus of the measurement, which is around 5 μm. Because this is not a confocal measurement, it is somewhat of an ill-posed problem to attempt to correlate area fraction with volume fraction, as the droplet dimensions along the gradient direction are not known. A crude geometrical argument for a two-dimensional slice of a three-dimensional ensemble of monodisperse spheres, however, gives the approximate relation $\phi \approx 4\varphi^{3/2}/3\pi^{1/2}$, where φ is the area fraction of droplets. Based on the measured (mean) area fractions obtained from the images, this simple formula gives $\phi = 0.20$, 0.35, and 0.75 for true volume fractions of 0.20, 0.40, and 0.80, respectively, ensuring that the procedure, although approximate, is consistent.
[21] E. Moses, T. Kume, and T. Hashimoto, Phys. Rev. Lett. **72**, 2037 (1994).
[22] See, for example, Y. W. Lee, *Statistical Theory of Communication* (Wiley, New York, 1960).
[23] P. Debye, H. R. Anderson, and H. Brumberger, J. Appl. Phys. **28**, 679 (1957).
[24] This asymmetry, although not immediately evident in the upper-left micrograph of Fig. 2, can be seen in the local director field in the lower-right panel. Some asymmetry of this type was invariably present in many of the images, although to varying degrees. The peaks are not artifacts, in the sense that the positions are reproducible and insensitive to the degree of asymmetry, which is controlled by slightly varying the angle between the axis of illumination and $\hat{\mathbf{y}}$. We note, however, that when $p(\theta)$ is broadly peaked around the vorticity direction ($\Theta = 0$), our data are not of sufficient quality to resolve any *true* higher-order peaks in the distribution, and Θ must be regarded as a cutoff in this case.
[25] E. Anczurowski and S. G. Mason, J. Colloid Interface Sci. **23**, 533 (1967).
[26] J. M. Rallison, Annu. Rev. Fluid Mech. **16**, 45 (1984).
[27] When the matrix phase is more elastic than the droplet phase, it can be argued (see E. K. Hobbie and K. B. Migler, Ref. 9) that the tendency for vorticity elongation is replaced by vorticity contraction, which might favor domains that are extended along the flow direction.
[28] G. Ver Strate and W. Phillipoff, J. Polym. Sci. Polym. Lett. **12**, 267 (1974); C. Rangel-Nafaile, A. B. Metzner, and K. F. Wissbrun, Macromolecules **17**, 1187 (1984).
[29] T. Hashimto and K. Fujioka, J. Phys. Soc. Jpn. **60**, 356 (1991); X. L. Wu, D. J. Pine, and P. K. Dixon, Phys. Rev. Lett. **66**, 2408 (1991).

[30] J. W. van Egmond, D. E. Werner, and G. Fuller, J. Chem. Phys. **96**, 7742 (1992).
[31] J. Yu *et al.*, Phys. Rev. Lett. **78**, 2664 (1997).
[32] E. K. Hobbie *et al.*, Phys. Rev. E **54**, R5909 (1996).
[33] Z. Shou and A. Chakrabarti, Phys. Rev. E **61**, R2200 (2000).
[34] A. I. Nakatani *et al.*, Phys. Rev. Lett. **79**, 4693 (1997).
[35] K. Krishnan, K. Almdal, W. R. Burghardt, T. P. Lodge, and F. S. Bates, Phys. Rev. Lett. **87**, 098301 (2001).
[36] H. Tanaka, Phys. Rev. Lett. **76**, 787 (1996); H. Tanaka and T. Araki, *ibid.* **78**, 4966 (1997).
[37] A. Bhattacharya, S. D. Mahanti, and A. Chakrabarti, Phys. Rev. Lett. **80**, 333 (1998).
[38] T. Taniguchi and A. Onuki, Phys. Rev. Lett. **77**, 4910 (1996).
[39] N. Toyoda, M. Takenaka, S. Saito, and T. Hashimoto, Polymer **42**, 9193 (2001).

LETTERS TO THE EDITOR

The Letters to the Editor section is divided into three categories entitled Notes, Comments, and Errata. Letters to the Editor are limited to one and three-fourths journal pages as described in the Announcement in the 1 January 2003 issue.

ERRATA

Erratum: "Shear-induced structure in polymer blends with viscoelastic asymmetry" [J. Chem. Phys. 117, 6350 (2002)]

E. K. Hobbie,[a] H. S. Jeon, H. Wang, H. Kim, D. J. Stout, and C. C. Han
National Institute of Standards and Technology, Gaithersburg, Maryland 20899

[DOI: 10.1063/1.1543144]

We recently discovered an error in Eq. (4) of the above paper. The correct equation is

$$\alpha(\hat{\mathbf{n}})^2 = \sum_{i=1}^{3} (\hat{\mathbf{n}}\cdot\hat{\mathbf{x}}_i / R_i)^2. \tag{4}$$

With this correction, the Fourier transform of Eq. (3) is then indeed Eq. (5), as stated in the text. The analysis and conclusions of the paper are unaffected. We apologize for this error and regret any confusion that it may have caused.

[a]Electronic mail: erik.hobbie@nist.gov